Journal of Geophysical Research: Atmospheres

RESEARCH ARTICLE
10.1029/2018JD029103

Special Section:
Bridging Weather and Climate: Subseasonal-to-Seasonal (S2S) Prediction

On the Harvest of Predictability From Land States in a Global Forecast Model

Paul A. Dirmeyer[1], **Subhadeep Halder**[2], **and Rodrigo Bombardi**[3]

[1]Center for Ocean-Land-Atmosphere Studies, George Mason University, Fairfax, VA, USA, [2]K. Banerjee Centre of Atmospheric and Ocean Studies, University of Allahabad, Allahabad, Uttar Pradesh, India, [3]Department of Geography, Texas A&M University, College Station, TX, USA

Key Points:
- The degree of potential predictability from soil moisture information that is realized as forecast skill has been quantified for CFSv2
- CFSv2 forecasts of temperature, humidity, surface fluxes, and boundary layer properties benefit from accurate soil moisture initialization
- CFSv2 forecasts of clouds and precipitation are likely unrealistically insensitive to soil moisture

Supporting Information:
- Supporting Information S1

Correspondence to:
P. A. Dirmeyer,
pdirmeye@gmu.edu

Citation:
Dirmeyer, P. A., Halder, S., & Bombardi, R. (2018). On the harvest of predictability from land states in a global forecast model. *Journal of Geophysical Research: Atmospheres*, *123*, 13,111–13,127. https://doi.org/10.1029/2018JD029103

Received 1 JUN 2018
Accepted 10 NOV 2018
Accepted article online 14 NOV 2018
Published online 4 DEC 2018

Abstract Various land surface treatments in a suite of subseasonal-to-seasonal forecasts are applied to diagnose the degree to which potential predictability from the land surface is harvested, where breakdowns occur in the process chains that link land surface states to atmospheric phenomena, and the role played by memory in the climate system. Version 2 of the Coupled Forecast System (CFSv2) is used for boreal summer simulations spanning 28 years. Four types of retrospective forecasts are produced: those where land surface initial states are from the same date and year as the initial atmosphere and ocean states; ensembles where initial land states come from different years than the atmosphere and ocean; simulations where soil moisture is specified from an observationally constrained analysis; and simulations where an alternative triggering mechanism for convection is employed. The specified soil moisture allows estimation of an upper bound for land-driven predictability and prediction skill in boreal summer. Realistic land initialization represents the best possible case with this model in forecast mode, while the simulations with initial land states from different years isolate the impact of atmosphere and ocean initialization on forecasts. Harvested predictability is calculated, and its relationship to memory of initial anomalies is estimated. The pathway of land surface information through the energy and water cycles to the atmosphere, and ultimately its effects on precipitation, is traced, showing a robust propagation of useful signal through land surface fluxes, near-surface meteorological states, and boundary layer properties, but largely disappearing at precipitation, implying problems with the convective parameterization.

Plain Language Summary The performance of the National Weather Service's operational climate forecast model is examined to see how the land surface, namely, moisture in the soil, affects the skill of forecasts. We estimate the potential skill derived from the best possible initialization and prediction of land surface states and how much of that potential skill can be realized by the current version of the forecast model. Additionally, we trace the signal of information in the model from the land surface into the atmosphere and find that while good soil moisture information greatly extends the duration of useful temperature and humidity forecasts, much information appears to be lost at the point in the model where clouds and precipitation are simulated. This result suggests that the model could be improved to make better use of land surface data to produce more skillful precipitation forecasts.

1. Introduction

There is great interest in predictions for the period of transition between deterministic short-term weather forecasts, which are dominated by evolution of the initial state of the atmosphere as a dynamic fluid system in continuous disequilibrium, and probabilistic seasonal to climate forecasts controlled by the slow manifold of ocean heat content evolution and its feedback on the atmosphere (National Academies of Sciences, Engineering, and Medicine, 2016). This appears to be an interval where variations in land surface states may have their greatest contribution to predictability (Dirmeyer et al., 2015). However, the land surface lacks operational near-real-time monitoring akin to what is in place for the atmosphere and ocean. Thus, unrealistic initialization of land surface states remains the norm for many weather and climate forecast systems (Vitart et al., 2017).

This "land gap" is a missed source of prediction skill. A chain of feedback processes through both the energy (thermodynamic) and water (hydrologic) cycles that connect variations in the land surface and atmosphere (Santanello et al., 2018). Recently, nonoperational data sets of land surface states have grown in number,

coverage, duration, and quality, allowing for preliminary investigations of the veracity of coupled land-atmosphere processes in weather and climate models (Cheruy et al., 2014; Dirmeyer et al., 2016, 2018; Levine et al., 2016; Trigo et al., 2015; Williams et al., 2016; Zeng & Yuan, 2018). These studies are beginning to suggest where things may be going amiss in coupled land-atmosphere model systems, which previously could undergo only very limited validation.

In the case of predictability derived from slowly varying (with respect to the atmosphere) land surface states, the baseline situation is some form of unrepresentative land surface initialization, such as from a climatological state (no interannual variability) or states that are effectively random with regard to the actual initial state of soil moisture and other land surface quantities. The second Global Land-Atmosphere Coupling Experiment (GLACE-2; Koster et al., 2010, 2011) was an initial multimodel attempt to quantify the impact of realistic land surface initialization on subseasonal forecasts. Among the 12 participating models, one third showed significant improvement in retrospective forecast skill, particularly for near-surface air temperature. However, two thirds of the models showed no improvement, suggesting there were other factors that encumbered them from realizing skill improvements. It was also found that improvements were strongest where a combination of high-density, high-quality observations went into producing analyses used to generate initial land surface states and where the coupling between land and atmosphere was strong (Koster et al., 2010, 2011). Thus, a combination of individual model properties and natural sensitivity of the atmosphere to variations in land surface states have been found to determine the impact of land surface initialization on model forecast skill.

Dirmeyer and Halder (2016, 2017) focused on one operational model, the National Centers for Environmental Prediction Coupled Forecast System version 2 (CFSv2; Saha et al., 2014). They examined how realistic land surface initialization affected skill in a range of variables, both of practical interest (e.g., near-surface temperature and precipitation) and that lie in the chain of processes (e.g., land surface fluxes and boundary layer height) that link land surface states to important meteorological phenomena like precipitation. The geographical variations in skill improvement largely reflected patterns of land-atmosphere coupling strength. However, there was a marked disconnection where improved skill was demonstrated in forecasting variations in surface fluxes, near-surface meteorological states, and atmospheric boundary layer properties, but not in precipitation. Perhaps due to the way precipitation processes are parameterized in CFSv2, land surface states appear to have little impact on forecast skill, even though significant correlations are found in reanalyses using the same basic modeling framework (Dirmeyer, 2013).

In this paper, we pursue further the potential causes of this apparent breakdown in the process chain linking precipitation to surface and lower tropospheric properties over land. We also attempt to quantify the upper bound of skill in CFSv2 hindcasts to evaluate predictability arising from land surface states, and establish the fraction of harvestable skill obtained by realistic land surface initialization, which is effectively the best that could be done in a real forecast situation. Section 2 describes the forecast model, experiment design, and data sets used for validation. This includes a novel means of forecast construction that seamlessly bridges the transition between weather and subseasonal time scales. Section 3 describes the duration of significant skill, amount of harvested skill, and the sources of skill in subseasonal CFSv2 forecasts. In section 4, we follow the process chains that are the feedback pathways from the land surface back to cloud and precipitation changes in order to diagnose model behavior. Conclusions are presented in section 5.

2. Models and Validation Data

CFSv2 is a fully coupled global ocean-atmosphere-land model used operationally by the Climate Prediction Center (CPC) of the National Centers for Environmental Prediction for forecasts out to 9 months, and for experimental forecasts as part of both the Subseasonal-to-Seasonal (S2S) Prediction Project (Vitart et al., 2017) and the Subseasonal Experiment (Kirtman et al., 2017). The components of CFSv2 as used in this experiment are version 2 of the Global Forecast System (GFSv2) atmospheric model at a horizontal resolution of approximately 0.9° (T126 spectral resolution) with 64 vertical levels and version 4 of the Modular Ocean Model (MOM4; Griffies et al., 2004) at a horizontal resolution of 1/2°, increasing to 1/4° meridionally at the equator and 40 vertical layers. A version of the Geophysical Fluid Dynamics Laboratory Sea Ice Simulator (cf. Saha et al., 2010) is coupled to MOM4. Noah version 2.7.1 (Ek et al., 2003) is the land surface model coupled to GFS, having four soil layers with interfaces at depths of 0.1, 0.4, 1.0, and 2.0 m.

GFSv2 uses the simplified Arakawa-Schubert (SAS) convective parameterization scheme (Hong & Pan, 1996; Pan & Wu, 1995). This scheme has long been suspected to be especially insensitive to land surface forcings (e.g., Zhang et al., 2011). Recent studies by Bombardi et al. (2015, 2016) have examined alternatives to the default convective triggering, including, as also examined here, an update to SAS that includes shallow cumulus (Han & Pan, 2011) and an alternative triggering criterion that is more physically based (Tawfik & Dirmeyer, 2014). The operational boundary layer scheme is that of Hong and Pan (1996) with an added background vertical diffusion term for enhanced mixing near the surface in stable regimes. The boundary layer scheme is also revised in the CFSv2 version with SAS updates, as described by Han and Pan (2011) and Bombardi et al. (2016).

Hindcasts cover the boreal warm season, with initial dates on the first day of April, May, and June for 1982–2009. Initial states come from the corresponding reanalysis: CFSR (Saha et al., 2010). The land states in CFSR are reset at 0000UTC each day from a parallel offline Noah simulation driven by surface meteorological forcing from the GFS data assimilation system but with precipitation from observed global analyses (Xie & Arkin, 1997; Xie et al., 2007) blended with 6-hourly precipitation generated by GFSv2. Land states include soil water and ice content, soil and vegetation temperatures, and snow mass—all other land properties are specified from fixed or seasonally varying (for vegetation) parameter sets. The CFSR Global Land Data Assimilation framework, which is derived from the NASA Land Information System (Peters-Lidard et al., 2007), is used to generate the 0000UTC land surface analyses at the same resolution as CFSR. The land surface analysis is said to be "semicoupled" to the atmosphere, preventing systematic errors from atmospheric model parameterizations from drifting water budget terms. There is no direct assimilation of land states in this system, but daily snow water equivalent analyses are generated from the Snow Depth Analysis Model (SNODEP) model of the Air Force Weather Agency (Kopp & Kiess, 1996) and after 1996 from the National Oceanographic and Atmospheric Administration Interactive Multisensor Snow and Ice Mapping System (Helfrich et al., 2007), which are blended with CFSR Global Land Data Assimilation-predicted fields each day to produce a smooth evolution of the snowpack. More details may be found in Saha et al. (2010).

For each of the 28 years with a particular initialization date, CFSR-analyzed states are interpolated to the CFS model resolution using code supplied as part of the model. Ensembles of 28 members are composed by choosing land initial conditions (ICs) from each of the 28 years. Thus, one member has the initial land states from the same year (Same-Year IC) that are consistent with the atmosphere and ocean states for that date and year, while the other 27 have the same atmosphere and ocean ICs but initial land states from the other 27 years (Different-Year IC). Additionally, a 29th ensemble member is generated for each date and year where the initialization is as in Same-Year IC, but soil moisture states are specified throughout the retrospective forecast from the land analysis described above (Same-Year BC).

Finally, a subset of years was chosen for short 2-week simulations with 3-hourly output to test the effects of convective triggering based on the heated condensation framework (HCF; Tawfik & Dirmeyer, 2014, Tawfik et al., 2015a, 2015b), as described in Bombardi et al. (2016). This was done because as mentioned in section 1, there is a breakdown in transfer of the predictability signal from land surface states from planetary boundary layer (PBL) properties, which are clearly improved by land surface initialization, to precipitation. Table 1 shows the configurations.

Here we describe the rationale by which comparisons between experiments may elucidate aspects of predictability arising from the land surface. The Different-Year IC cases provide, in the mean, a quantification of skill arising from atmospheric and ocean initialization alone. Comparing the Same-Year BC case with the set of 27 forecasts from Different-Year IC with the corresponding initial month provides an upper bound of realizable predictability from the best possible land surface simulation. It should be noted that this is not the absolute best that may be done, as (1) the meteorological data that are used to drive the Noah land model are of varying quality over different places around the globe; (2) Noah is not a perfect model in representing the evolution of land surface states; and (3) GFSv2 likewise does not perfectly represent the atmospheric sensitivities to land surface variability. Given these limitations, Same-Year BC versus Different-Year IC provides the maximum idealized potential skill from land states in this model configuration. Same-Year IC versus Different-Year IC quantifies the harvested skill in actual forecast mode, as specified states are not an option in real-time forecasting. Same-Year BC versus Same-Year IC cases provide an estimate of the unharvested skill, noting that a perfect land forecast is not possible, so some of the unharvested skill is in fact unharvestable.

Table 1
Model Experiments With CFSv2

Name	Initialization	Ensemble size	Atmosphere and ocean ICs	Land	Duration	Model physics
Same-Year IC	1 Apr, May, Jun: 1982–2009	1 per IC	CFSR	CFSR ICs	≥4 months	Operational
Different-Year IC	1 Apr, May, Jun: 1982–2009	27 per IC	CFSR	CFSR ICs from other years	≥4 months	Operational
Same-Year BC	1 Apr, May, Jun: 1982–2009	1 per IC	CFSR	CFSR prescribed soil moisture	≥4 months	Operational
NoHCF	15 July: 1998–2010	4 per IC	CFSR	CFSR ICs	2 weeks	New SAS and shallow Cu
HCF	15 July: 1998–2010	4 per IC	CFSR	CFSR ICs	2 weeks	New SAS and shallow Cu + HCF trigger

Note. Same-Year IC, NoHCF, and HCF have land initial states from the same year as the atmosphere and ocean ICs, Different-Year IC has land initial states from all years other than the year of the atmosphere and ocean ICs, and Same-Year BC has time-varying land states prescribed from CFSR for the same year as the atmosphere and ocean ICs. CFSv2 = Coupled Forecast System version 2; IC = initial condition; HCF = heated condensation framework; NoHCF = no heated condensation framework; CFSR = Coupled Forecast System reanalysis; SAS = simplified Arakawa-Schubert; BC = boundary condition.

Validation data come from gridded observational data sources for near-surface air temperature and precipitation and from reanalyses (CFSR) otherwise. The CPC global gridded daily temperature analysis has been acquired from the National Oceanographic and Atmospheric Administration Earth System Research Laboratory (see the Acknowledgments). The CPC unified gauge-based precipitation analysis (Chen et al., 2008; Xie et al., 2007) provides daily gridded precipitation totals for model validation.

Daily mean model and validation data are used to estimate coupling metrics and to perform process-based model evaluation in section 4. Validation of model forecast skill is performed on a time average over a window that varies as a function of forecast lead. This weighting takes a form based on a Poisson function (Ford et al., 2018) such that as forecast lead times get longer, the averaging window becomes wider. The functional form for a weighted time-average forecast $\boldsymbol{F}_{\lambda}$ of variable $\boldsymbol{X}$ at a specific lead λ days is $\boldsymbol{F}_{\lambda}=\frac{\sum_{k=1}^{N}\boldsymbol{W}_{\lambda,k}\boldsymbol{X}_{\lambda}}{\sum_{k=1}^{N}\boldsymbol{W}_{\lambda,k}}$ with weights, where sums are totaled over all leads λ in the forecast. The Poisson function has a value at $\boldsymbol{k=0}$, which corresponds to including the initial state (analysis) as part of the forecast. This is valid to do operationally, but because we are concerned about the model forecast behavior, we leave out the weight for $\boldsymbol{k=0}$ and renormalize the remaining weights $\boldsymbol{W}_{\lambda,\boldsymbol{k}}$, so they sum to 1. At very short leads, the forecast is heavily weighted to the day of validation like a typical deterministic weather forecast. As the forecast lead extends beyond a week or so, the distribution of weights spreads and flattens into a centered average with an approximately normal distribution, as the upper limit of a Poisson distribution is a Gaussian distribution. This provides a seamless transition to classical monthly and seasonal climate forecasts but also means that the forecast and validation fields become smoother with lead time, progressively losing contributions from short-term variations. It also means that the observed state for any particular validation date also varies with forecast lead time, which introduces some complexity in, for instance, calculating climatologies for the purpose of determining anomalies (which also vary with lead time in this approach).

3. Model Performance and Predictability

We assess skill by the anomaly correlation coefficient (ACC) calculated between model forecast and observed (or reanalysis) fields relative to the 28-year means, with the Poisson weighting applied to forecasts at various leads. Using this metric, we quantify the effect of the different initialization strategies in the multimonth forecasts, including specification of soil moisture throughout the retrospective forecast period, by assessing the duration from the start of the forecast over which significant skill is maintained through the forecast period. At the 95% confidence level, duration of skill is thus defined as the number of days the forecast ACC remains above 0.374.

3.1. Duration of Skill

Our expectation is that the Different-Year IC forecast suite should have the shortest duration of skill, and Same-Year BC cases should result in the longest duration. Specifics depend on several factors, including the natural predictability arising from land-atmosphere coupling (which varies in space and time), the quality of the soil moisture analysis (which is also spatially variable), and the model's ability to represent the

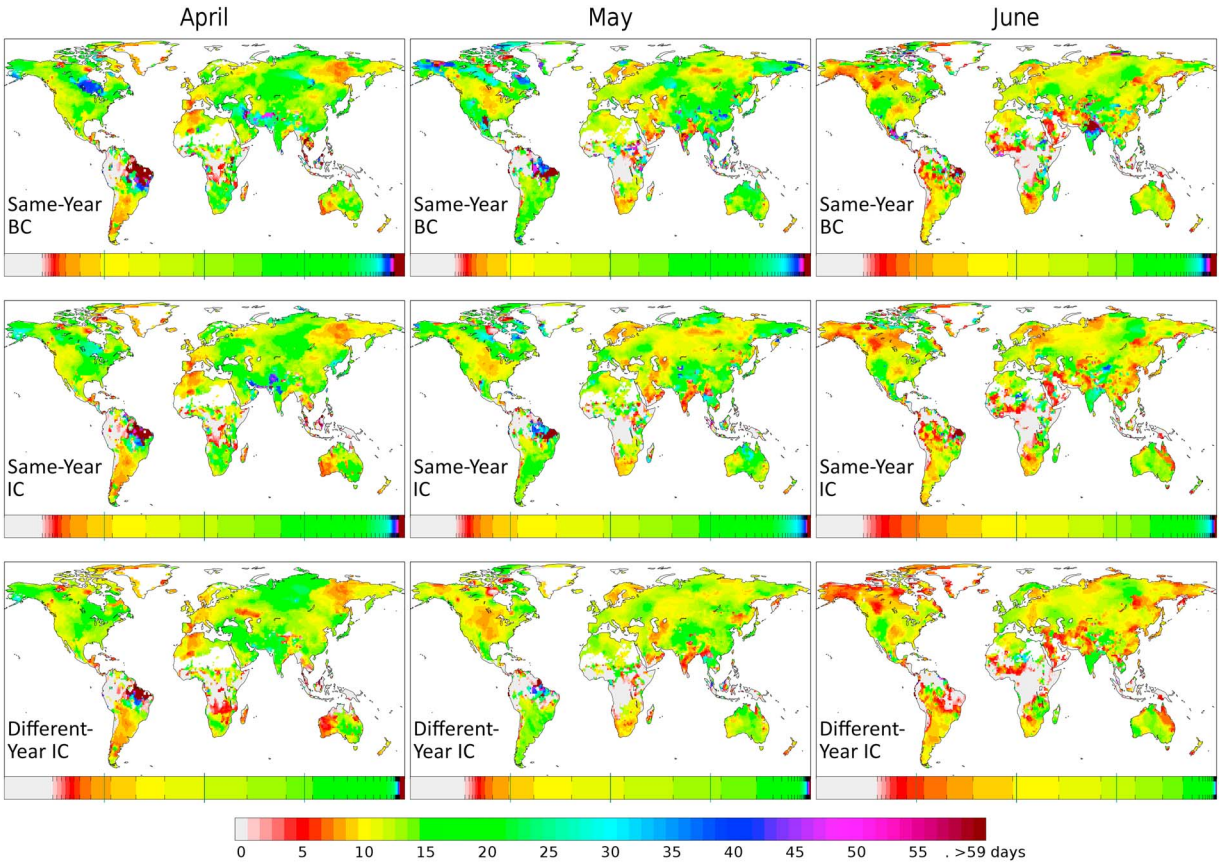

Figure 1. Duration of significant skill (last day from initialization on the first day of indicated month when interannual anomaly correlation coefficient significance remains better than $p = 0.05$) for 2-m air temperature for each of the three cases: (top row) Same-Year BC; (middle row) Same-Year IC; and (bottom row) Different-Year IC. Color bar beneath each panel shows fraction of land mass in each category (proportional to width of color), and green vertical marks denote quarters of total area. IC = initial condition; BC = boundary condition.

processes that link land and atmosphere. Areas with very small soil moisture variability, having a daily standard deviation of top 10-cm volumetric soil moisture <0.005, are masked out in this analysis (mainly over the Sahara), as are regions with permanent ice cover.

Figure 1 gives an indication of the variation in skill for 2-m air temperature from forecasts initialized at the beginning of April, May, and June for the three different treatments of soil moisture. The color scale below each map panel is a histogram showing the fraction of land area in each range of skill duration, with vertical lines at the 25%, 50%, and 75% levels for visual reference. There is a general shortening of the duration of skill as the forecast initial dates progress from April to June. The tropical maritime influence of Atlantic sea surface temperatures on temperatures over the eastern Amazon is apparent and is strongest in April. Elsewhere, the Poisson-weighted duration of significant skill is rarely longer than about 3 weeks, with a median of 10–14 days depending on month and initialization strategy. There is a lengthening of skill duration as the forecasts progress from randomized initial land states to realistically initialized to specified soil moisture, with some of the largest impacts along the snowmelt front at high northern latitudes and in some of the monsoon onset regions. Maps for other validated fields are shown in the supporting information as Figures S1–S3.

Global statistics for a number of variables are summarized in Figure 2. The disparity between percentage area improved and degraded indicates the degree to which the quality of the soil moisture fields has an impact on forecast skill. Of course, the skill of soil moisture itself is very sensitive, but surface latent heat flux (LHF) and sensible heat flux (SHF) are also sensitive. The positive impacts weaken somewhat but are still clear in 2-m temperature, humidity, and height of the daytime boundary layer. Precipitation is conspicuously insensitive, as has been noted before (cf. Dirmeyer, 2011; Dirmeyer & Halder, 2016, 2017). This result is examined further below and motivates inclusion of the HCF and NoHCF simulations in the analysis in section 4.2.

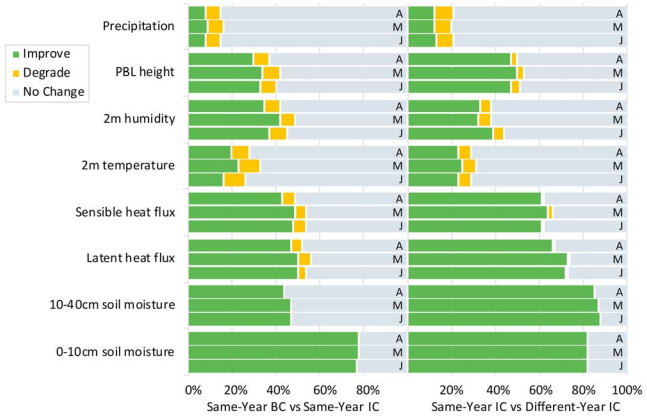

Figure 2. Percentage of ice-free land area of improvement or degradation in skill for the indicated variables and initialization months (A = April, M = May, J = June; skill threshold defined as ±1.0 standard deviations of the local interannual variability of ensemble mean skill in the Different-Year IC case). IC = initial condition; BC = boundary condition; PBL = planetary boundary layer.

Figure 3 illustrates the impact of the various treatments of soil moisture on the atmosphere as a function of forecast lead. The maps at the top of the figure show the number of days on average that the Poisson-weighted retrospective forecasts initialized on 1 May remain statistically significant, as was shown in the middle panel of Figure 1 for the specific case of near-surface temperature. The panels below show the cumulative distribution function of the fraction of skillfully forecast global land area (sans ice-covered areas or regions of very low soil moisture variability) as a function of forecast lead for the three classes of forecasts. For air temperature, skillfully predicted area drops sharply after about a week. The improvement by using realistic land surface initialization is immediate, and its impact is greatest between 10 and 20 days. Specified soil moisture improves skill further and extends it particularly after 2 weeks. For near-surface humidity the peak impact of realistic land surface initialization occurs sooner but is more pronounced. Specified soil moisture greatly increases the area of skillful forecasts after day 5 and extending throughout the duration of the forecast. The impact on the prediction of the depth of the PBL is even more profound, being greatest between 3 and 7 days for realistic land initialization, when the increase in skillful area reaches 30% of global land area. However, the effect on precipitation forecasts is clear but minimal, peaking between days 8 and 12 but increasing the area of skillful predictions by at most a few percent of global land area.

3.2. Harvested Skill

The spatial distribution of the changes in the duration of skill for near-surface air temperature shown in Figure 1 is presented in Figure 4. The first row shows the change from Same-Year IC to Same-Year BC, and the middle row shows the change from Different-Year IC to Same-Year IC. Realistic initialization improves

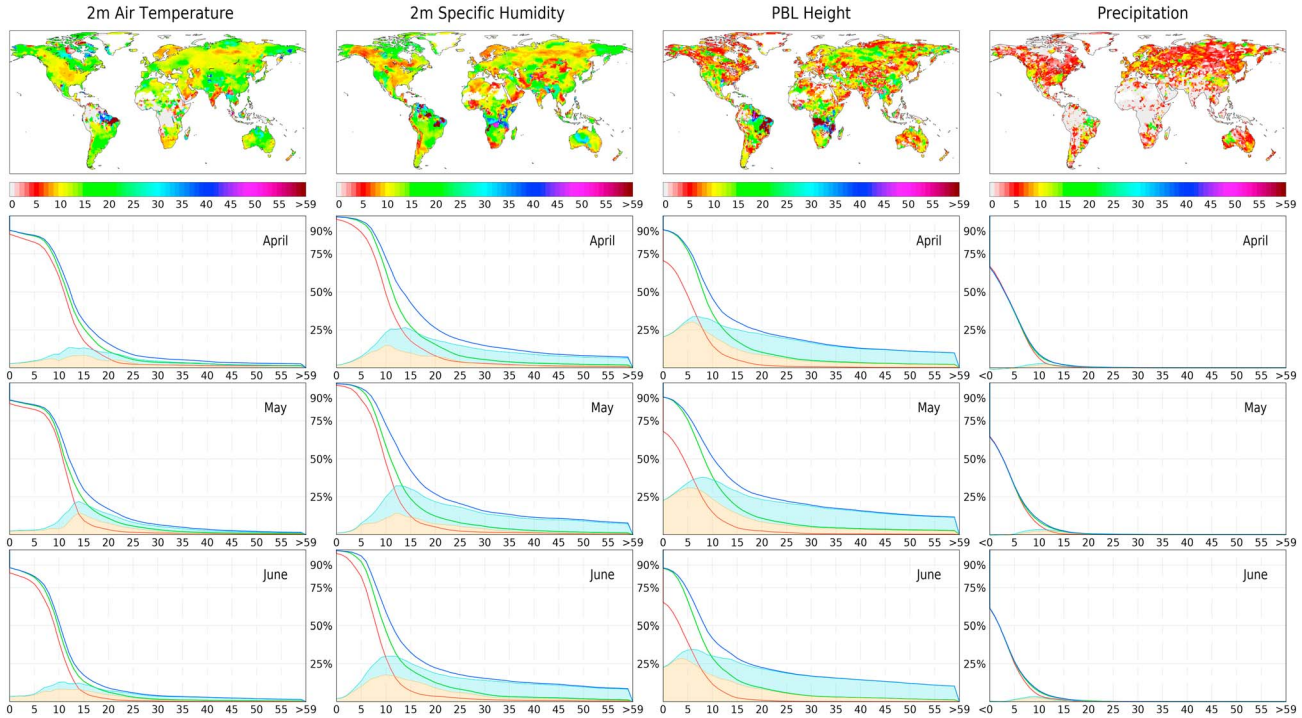

Figure 3. Top row is as in Figure 1 for 1 May Same-Year IC for the indicated quantities; subsequent rows show the fraction of land area exhibiting significant skill as a function of forecast lead time with Same-Year BC (blue), Same-Year ICs (green), and Different-Year ICs (red). Shaded curves show the difference between green and red curves (tan) and between blue and green curves (pale blue). IC = initial condition; BC = boundary condition; PBL = planetary boundary layer.

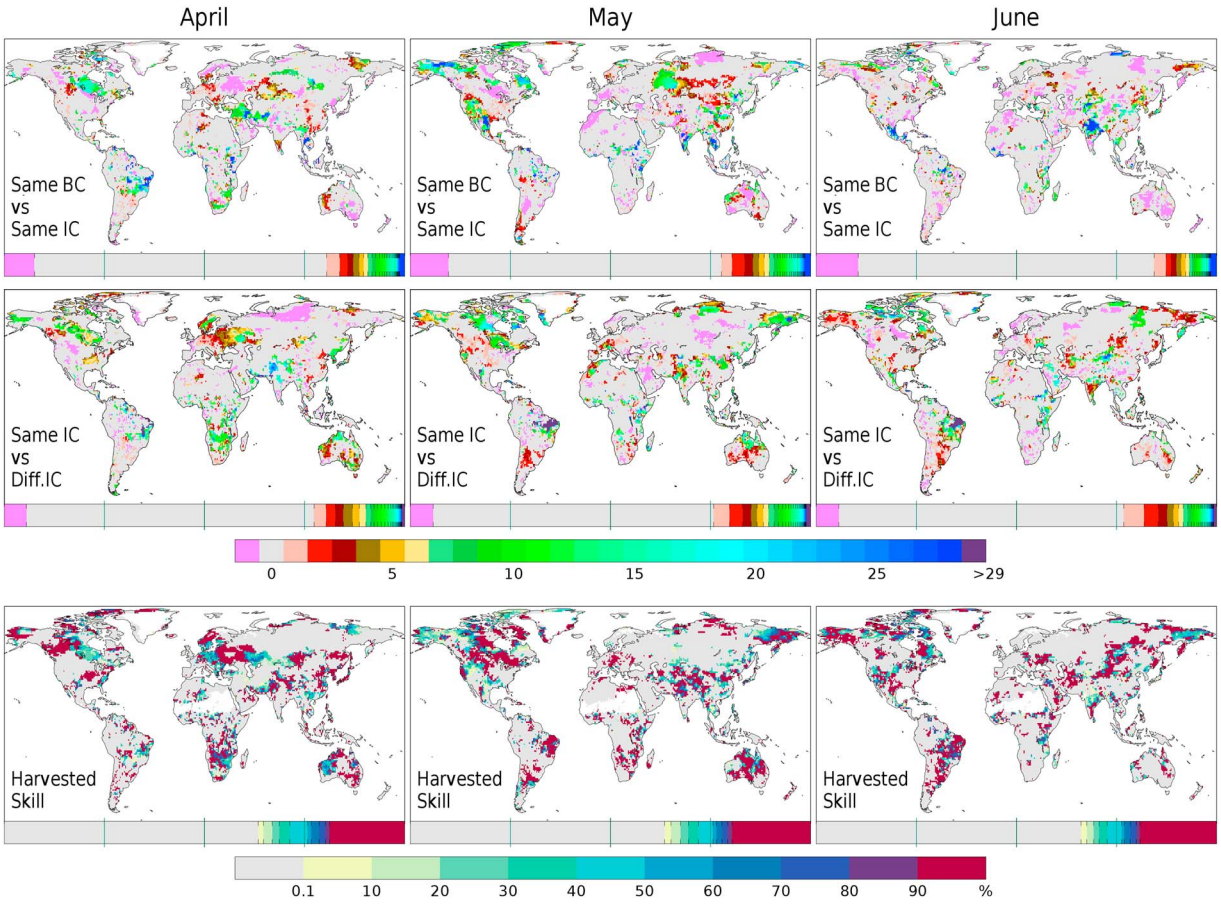

Figure 4. For forecasts initialized on the first day of the indicated months (each column), the increase in days of significant skill in 2-m air temperature between suites of forecasts; (top row) Same-Year BC minus Same-Year IC and (middle row) Same-Year IC minus Different-Year IC. Magenta indicates a decrease in the duration of skillful forecasts, and the zero or no-change category in gray includes all areas where the magnitude of changes are less than ±1.0 standard deviations of the local interannual variability of ensemble mean skill in the Different-Year IC case. The bottom row shows the percentage of harvested potential predictability (middle row divided by sum of top and middle rows). Color bar beneath each panel is as in Figure 1. IC = initial condition; BC = boundary condition.

skillful forecast duration over 22–25% of land areas, while about 6% of areas show degraded skill. For temperature and most other variables (quantified in Figure 2), improvements going to specified soil moisture are more limited in area and degradations are somewhat more common.

The percentage of skill that is harvested can be estimated as the ratio of difference in the change of skill going from Different-Year IC to Same-Year IC (realized skill) divided by the difference in the change between the two. The bottom panels of Figure 4 show this, except that when either of those changes is negative, the harvested skill is zero. In each month, about 30–35% of the land area sees extended duration of skill, with about 20% seeing all the potential skill realized. It should be kept in mind that there are several possible reasons that little or no skill is realized over so much of the globe. These include the following: (1) the model as formulated lacks the ability to realize potential skill that is harvestable from the land ICs; (2) the quality of the initial land states is poor; (3) there is realizable skill, but the sample size from these forecasts is too small to discern it; and (4) there is no inherent predictability to be realized from the land surface. On the other side of the coin, some of the colored areas may be false positives, particularly as a result of the limited sample size. This is most likely at high latitudes where baroclinicity and internal variability of atmospheric temperature are high. Regions known from previous research to be "hotspots" of land-atmosphere coupling during these periods are more likely to be genuine, such as over central North America, southern and central Asia, and eastern Europe, as well as much of Africa, Australia, and South America south of the Amazon basin. For comparison, Figures S4–S6 show the same analysis for 2-m specific humidity, PBL height, and precipitation.

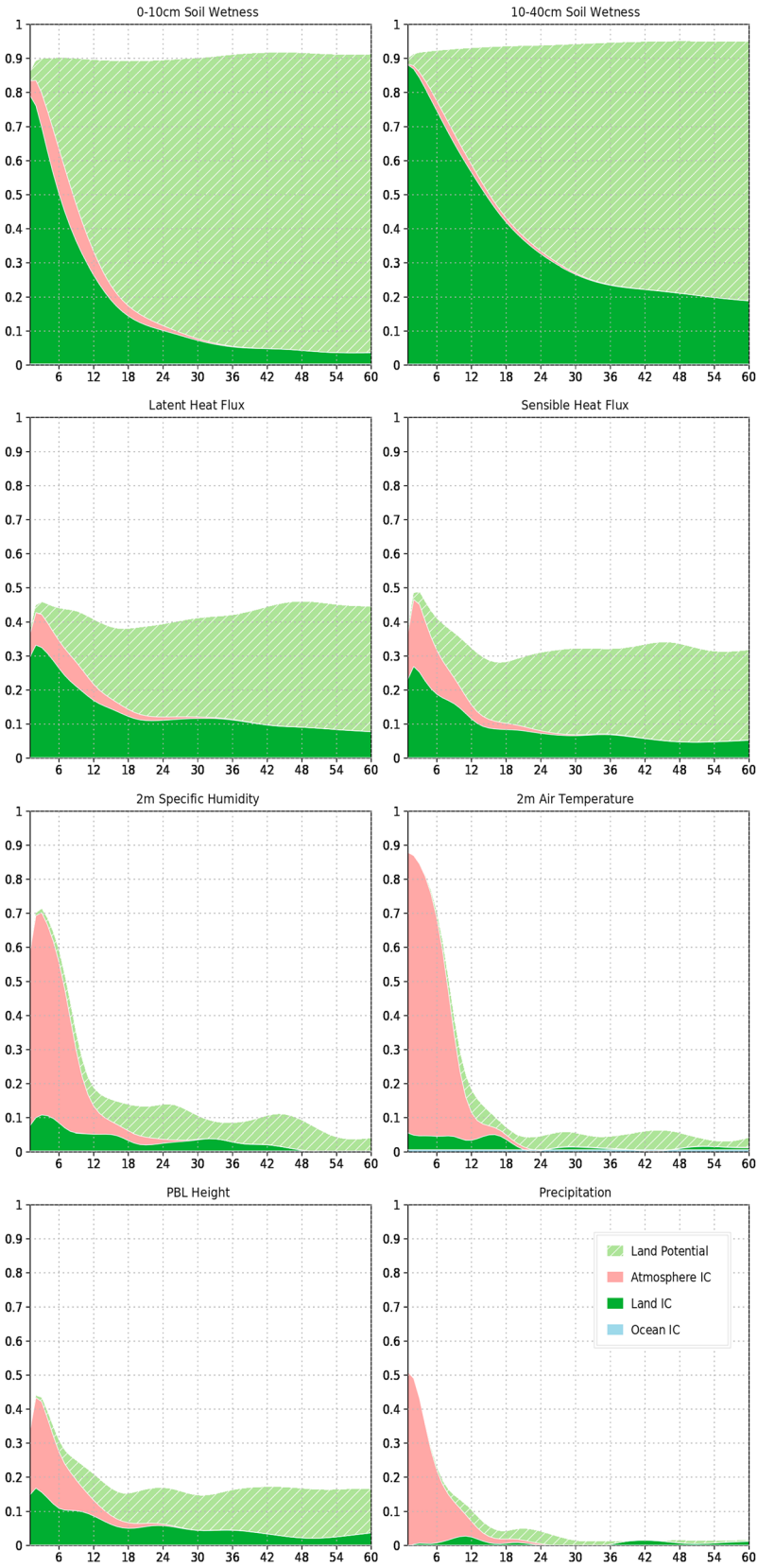

Figure 5. Fraction of ice-free land area showing significant forecast skill as a function of lead time (abscissa; days); determination of the sources of skill is described in the text. IC = initial condition.

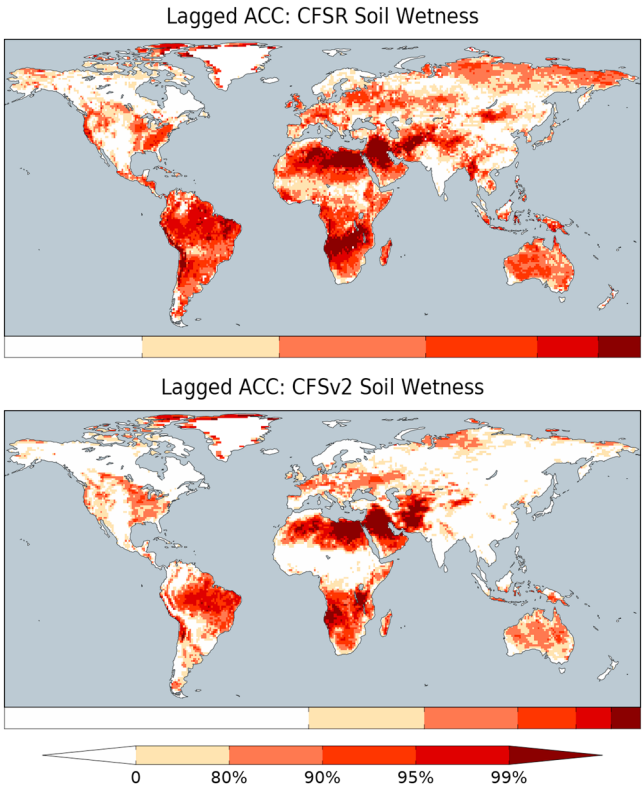

Figure 6. Comparison of the lagged autocorrelation of top 10-cm soil wetness during JJA between pentad 1 and pentad 3 (mean of days 1–5 of month versus days 11–15 of same month) for the (top) CFS reanalysis and (bottom) CFSv2 forecasts initialized on 1 June with right land states; calculations span 1982–2009. Colors indicate significance levels; the color bar beneath each panel indicates the fraction of land mass in each category (proportional to width of color band). JJA = June-July-August; ACC = anomaly correlation coefficient; CFS = Coupled Forecast System; CFSR = Coupled Forecast System reanalysis; CFSv2 = Coupled Forecast System version 2.

3.3. Impact of Initialization

The evolution over time of the impact of each initialization and boundary condition (BC) element can be assessed. The impact of land initialization can be estimated from the difference between the skill in retrospective forecasts with Same-Year versus Different-Year ICs. The impact of sea surface temperatures is assessed from the time average of the ensemble with randomized land states after the impact of atmospheric initialization has died down. We average the forecast skill from days 31 to 60 and apply that as a constant value through the subseasonal forecasts. The atmospheric impact is that from the Same-Year IC forecasts minus the separate land and ocean impacts described above. Finally, the idealized upper bound for land surface prediction skill is the difference between Same-Year BC and Same-Year IC cases.

We average the forecast skill (ACC) of the indicated variables with Poisson weighting in Figure 5 over North America between 30 and 49°N for each of the first 60 days of the suite initialized on 1 May. The ordinate shows the ACC contributed by each component. Obviously, soil moisture skill is high when it is realistically initialized, remains high when it is specified (indicated as the "land potential" above other sources), and has very little contribution from atmospheric or ocean initialization. The lack of perfection for soil moisture variables in Same-Year BC cases arises from the fact that model output is based on averages after the completion of each model time step when soil moisture is specified at the start of each time step; the main deviations are in rainy areas. Atmospheric initialization is important for temperature, humidity, and precipitation and steeply degrades beyond weather time scales. Land initialization is of comparable importance for surface heat fluxes and PBL development as atmospheric initialization at short time scales yet persists much longer to become dominant after the first week. The potential suggested by specified land states maintains high skill for surface fluxes throughout the first 2 months and also remains a significant factor for PBL height and near-surface humidity. Ocean initial state contributions during boreal summer are essentially nil; since there are no separate experiments separating atmosphere and ocean initialization, any skill at day 60 in the Different-Year IC ensemble mean is presumed to arise from the ocean.

There is evidence that the influence of initial states in CFSv2 simulations is shorter than what one finds in nature (cf. Dirmeyer, 2011). This can be seen by comparing the lagged autocorrelation of soil moisture between simulations and the CFSR, in which land surface states are derived by running the same Noah land surface model uncoupled from the atmospheric model, driven by observed surface meteorology. Figure 6 provides a consistent comparison of soil moisture memory, following the twice-removed pentad methodology of lagged autocorrelation of Koster et al. (2003) to minimize the spurious contribution of short-term synoptic events to apparent subseasonal memory. This reduced persistence of initial land anomalies in CFSv2 simulations must originate from the atmospheric model. Figure 7 shows that lagged autocorrelations of precipitation in CFSv2 are also weaker than what gridded observed precipitation products suggest. The greater "noise" content of model precipitation leads to reduced potential impact of land surface states on forecasts. The large discrepancy over Africa is particularly noteworthy.

4. Feedback Pathways

Given a theoretical basis for process linkages among terms in the feedback chain linking the land surface back to the atmosphere, correlations are a handy tool to assess the strength of linkages. Among three variables, correlations can be used to deduce partial correlations (Olusegun et al., 2015; Thomas & O'Quigley, 1993), further constraining the relationships and allowing a clearer determination of genuine cause-effect

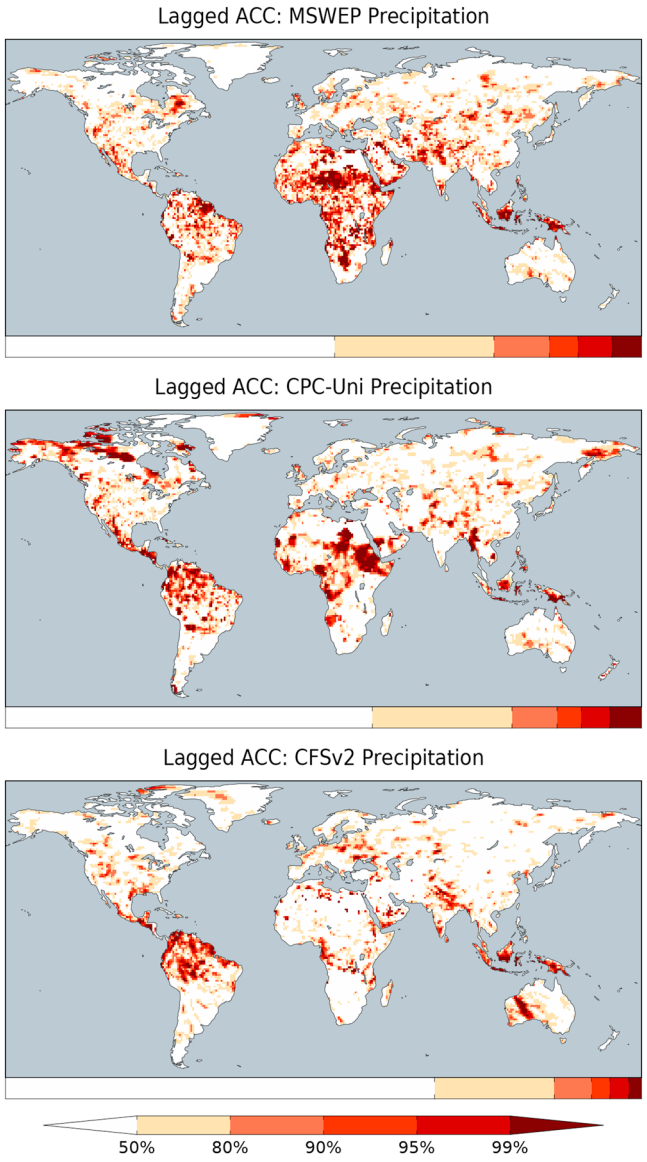

Figure 7. As in Figure 6 for precipitation: (top) multisource weighted-ensemble precipitation (MSWEP); (middle) Climate Prediction Center (CPC) Unified, and (bottom) Coupled Forecast System version 2 (CFSv2) forecasts. ACC = anomaly correlation coefficient.

relationships from spurious ones. A thorough assessment among prognostic and diagnostic model variables in the feedback pathways from land to atmosphere is summarized here. We then pursue evidence of a possible breakdown in the linkage between boundary layer properties and the triggering of clouds and convection by examining the impact of an alternative parameterization for convective initiation.

4.1. Partial Correlations

Many interesting features can be discerned from correlations among triads of variables; partial correlations reveal where one variable may be suppressing or enhancing correlations estimated between the other two variables. Here we focus on those sets of variables in the atmospheric leg of land-atmosphere coupling processes.

The first example is the set consisting of convective cloud cover (CCC), moist static energy (MSE) calculated from 2-m states, and surface LHF. All three of these terms tend to correlate strongly with one another over most of the globe during June (Figure 8). Looking in detail, LHF correlates positively to MSE over most locations. This indicates the direct contribution of LHF to moistening the lower troposphere, increasing the λq term. Negative values are seen primarily over Northern Hemisphere regions that have a winter rainy season, Arctic coastal regions, and scattered regions of the Southern Hemisphere. Strong positive correlations exist over the tropics, monsoon regions, and much of the midlatitudes of the Northern Hemisphere. The correlation between MSE and CCC is positive nearly everywhere, with the strongest correlations over areas including the deep tropics, southeastern Asia, much of Mexico, and the eastern seaboard of North America. The problem of overly robust transpiration over agricultural areas described by Roundy et al. (2014) is evident as the negative correlation areas between LHF and CCC over central North America, much of eastern China, and across Europe. This is symptomatic of an energy-limited condition at the land surface that is probably unrealistic in this model. Otherwise, the strong positive correlations linking LHF and CCC are again over much of the remainder of North America, the deep tropics, and monsoon areas (although not strong over West Africa) and in a band from northern Europe to the Amur basin.

When we control for the effect of MSE, nearly everywhere, the correlation between LHF and CCC drops. The impact is strongest over the tropics, Southeast Asia, monsoonal Mexico, and South Asia, and much of eastern North America, with a broad area of moderate impact over central and eastern Europe. The implication is that in these regions, there is a pathway through MSE by which surface LHF positively impacts convection. It is noteworthy that the regions of North America correspond well to the areas of strong triggering feedback strength found by Findell et al. (2011). The other side of the coin is that locations of strong positive correlation between LHF and CCC not reduced by controlling for MSE must be related for other reasons. For example, over the western United States it is more likely that convective precipitation in this generally dry region contributes to increased evaporation, and the feedback pathway is not in place.

Figure 9 shows the global relationships in the form of scatter diagrams. The strong positive correlation among the three terms is evident as most points lie in the upper right quadrant and are colored red. The scatter is then colored by values of two different aridity indices, one based on precipitation and one on evapotranspiration (ET). Generally humid regions correspond to those where LHF correlates positively to MSE. In arid regions, the correlations in both links are generally weak. Where ET approaches its potential rate, there

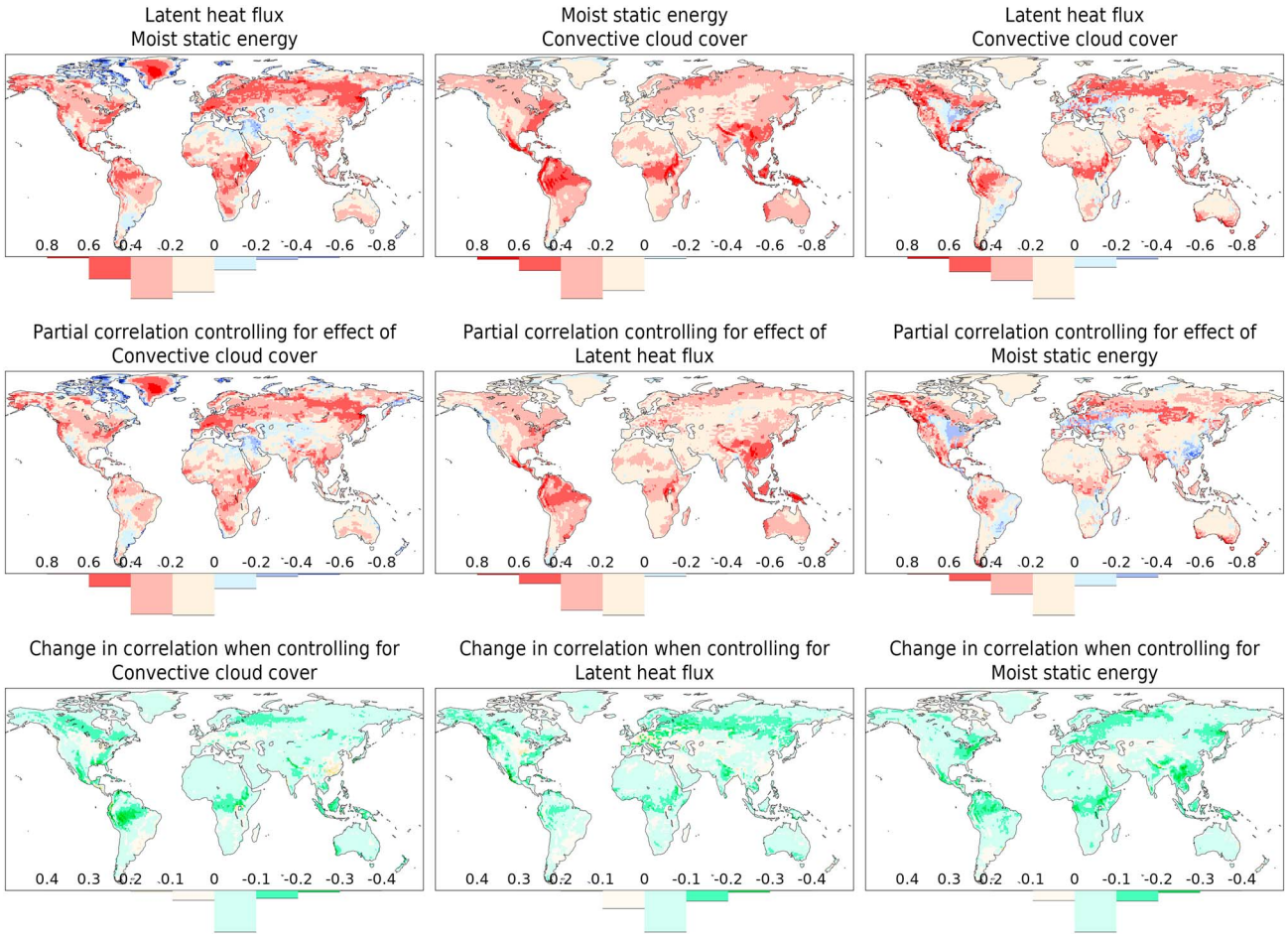

Figure 8. Forecasts initialized with right land states on 1 June 1982–2009, temporal correlations of daily means among surface latent heat flux, 2-m moist static energy, and convective cloud cover as indicated in the titles of each panel: (top row) simple correlations, (middle row) partial correlations controlling for the indicated variable, and (bottom row) the difference. Color histograms under each panel show the proportion of land area in each interval.

tends to be no correlation between MSE and CCC except when the relationship between LHF and MSE is strong and positive.

The second example is a dry feedback pathway from SHF to PBL height to CCC. SHF is the process by which the daytime boundary layer heats, fueling its growth. As a result, SHF correlates strongly with the height of the PBL over most of the globe (Figure 10), except some desert areas, Southern Hemisphere (winter) midlatitudes, and the regions where crops are exhibiting too much ET, which all have negative correlations. CCC is almost universally negatively correlated with both SHF and PBL in CFSv2. This is contrary to the notion of a dry-soil advantage in semiarid and arid regions, where deep boundary layers are most conducive to triggering clouds and convection (Findell & Eltahir, 2003; Roundy et al., 2013; Taylor et al., 2012). This inability to represent convection over hot dry ground is a characteristic of the convective parameterizations in many atmospheric models (e.g., Gentine et al., 2013; Hohenegger & Stevens, 2013; Zhang et al., 2017).

Setting that problem aside and looking at humid summertime and tropical regimes, the anticorrelation between PBL and CCC makes sense as a reflection of the paramount role of moisture—a moist atmosphere will have a lower cloud base, which acts to cap the depth of the PBL. Clouds also suppress surface sensible heating by reducing downward shortwave radiation, which acts as another factor in the negative correlation, exemplified directly in the rightmost column, and explains the apparent role of CCC in enhancing the positive correlations between SHF and PBL height when we account for the cross-correlations among these three terms. Meanwhile, much of the anticorrelation between SHF and CCC in the tropics and monsoon regions is directly attributable to the pathway through boundary layer growth.

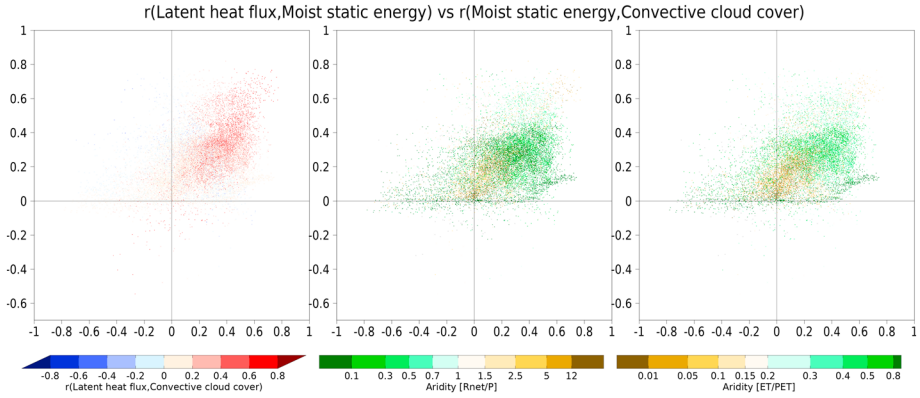

Figure 9. Information in the top left and top center panels of Figure 8 presented as a scatter diagram (each mark is one land model grid cell), colored by three quantities as indicated in the color bars. (left) Correlation shown in the top left panel of Figure 8, (middle) aridity defined as ratio of net radiation to precipitation (expressed as energy by multiplying by the latent heat of condensation), and (right) aridity expressed as ratio of evapotranspiration (ET) to potential evapotranspiration (PET).

4.2. Convective Parameterization

Because the breakdown in the linkage along the land-atmosphere feedback pathway appears to occur at precipitation, we examine simulations from Bombardi et al. (2016) that employed the convective trigger based

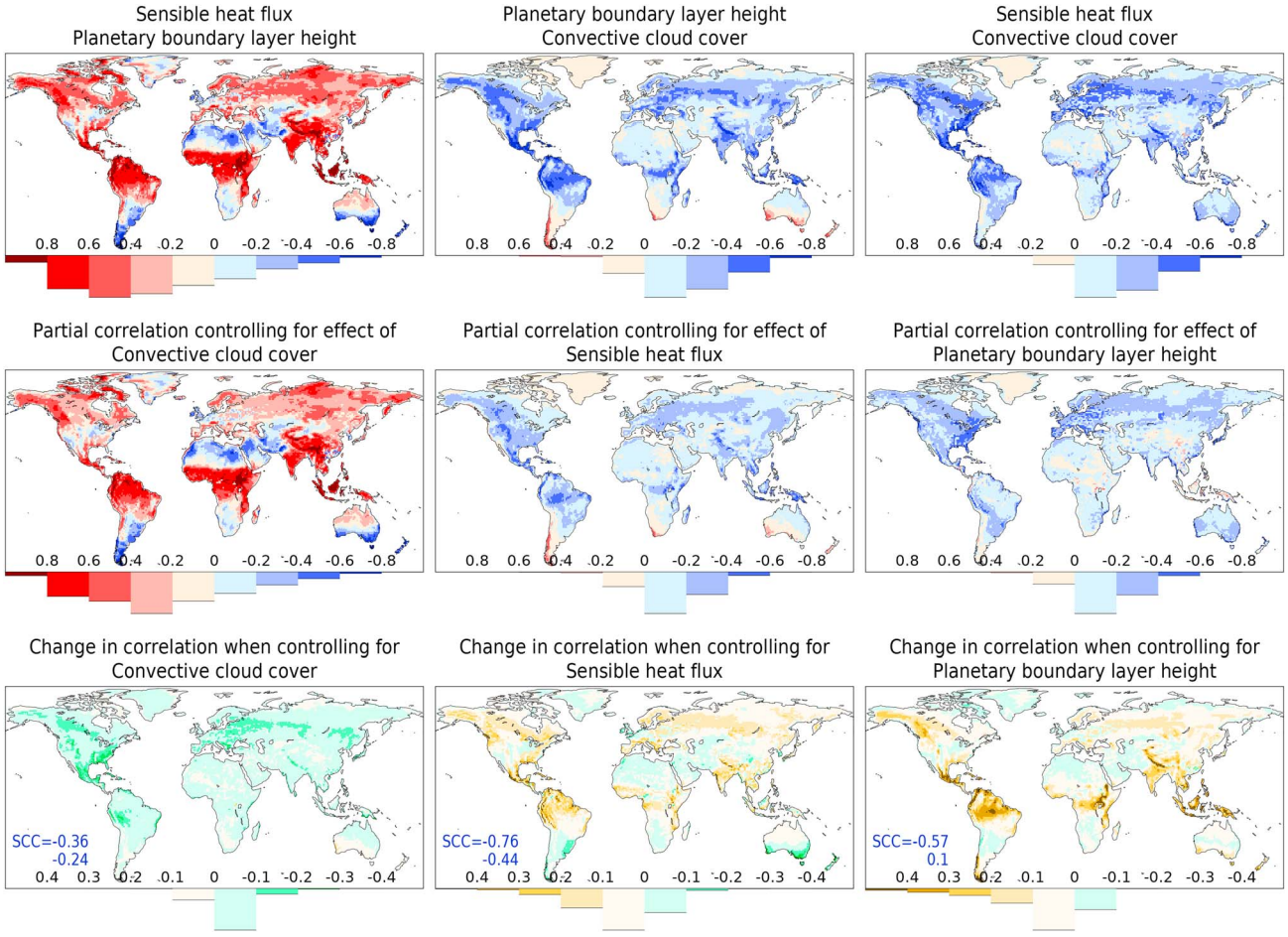

Figure 10. As in Figure 8 for correlations among surface sensible heat flux, boundary layer height, and convective cloud cover.

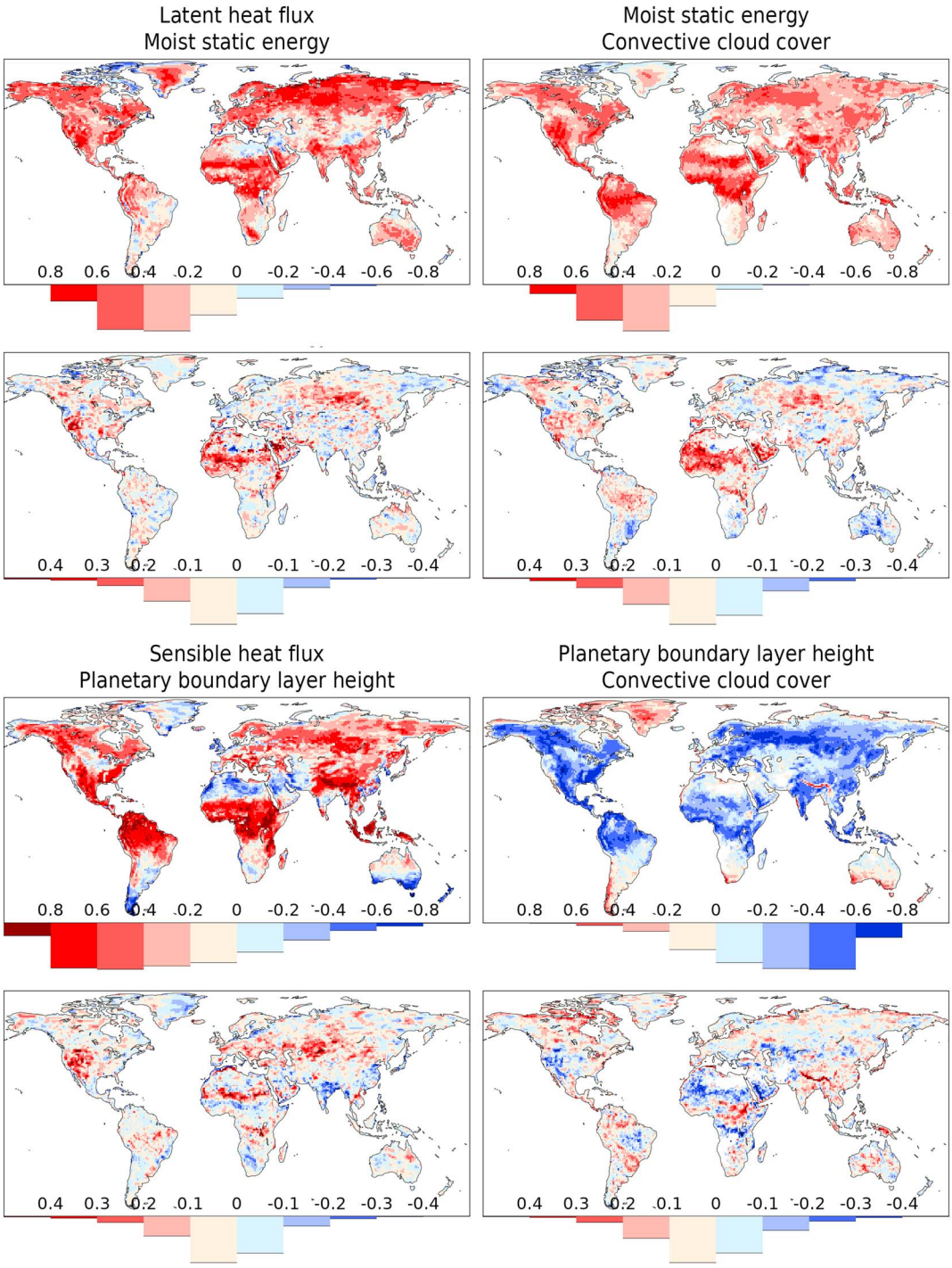

Figure 11. (top) Four pairs of panels showing the temporal correlations between variables indicated and (bottom) the change in correlation when the heated condensation framework (HCF) convective triggering mechanism is implemented. The top panel in each pair is not identical to the corresponding panels of Figures 8 and 10 because these forecasts were initialized on 15 July for a different set of years.

on the HCF of Tawfik and Dirmeyer (2014). The main difference is that HCF permits convection when there is sufficient heating for a well-mixed boundary layer to achieve saturation at its top, based on the evolving profiles of temperature and humidity. This relates triggering to the ability to overcome convective inhibition, which is in contrast to the convective parameterizations in CFSv2, wherein a necessary condition for both shallow and deep convection is that the level of free convection be within 120–180 hPa above the level of

maximum MSE. This default condition is replaced by the HCF condition in the HCF simulations, allowing a more realistic buildup of energy; other aspects of the shallow and deep convective parameterizations are unchanged.

Figure 11 shows that the impact of the HCF-based convective triggering in coupling land surface fluxes to convective cloud formation is mainly found in semiarid regions. Top panels show the water cycle pathway, linking surface LHF to MSE to convective cloud. Both of these links are manifested as mostly positive correlations except in the most arid regions and parts of the Arctic. Changes from the control case tend to expand and enhance these positive linkages into more arid locations like the Sahel, southwestern North America, and the transition areas between the central Asian deserts and Siberia.

The thermal pathway links surface SHF to growth of the boundary layer to cloud formation. The first link is mostly positive except over deserts, as with the water cycle links. However, there is generally an inverse relationship between PBL height and convective cloud formation, reflecting the fact that more humid air has a lower lifting condensation level that can be reached by a shallower boundary layer. Again, the greatest impact of the HCF triggering is over the semiarid regions, this time extending toward eastern Europe and appearing in some Southern Hemisphere dry-season regions.

In both pathways, HCF serves to bolster the linkages between land surface fluxes and convection, although the impacts are not widespread. Skewness is apparent in the histograms for each of the changes in correlation. To assess their significance, for each coupling pair of variables, we performed a Monte Carlo sampling from within the 104 HCF and NoHCF simulations dividing ensemble members randomly into two pairs of 52 and calculating the difference histograms 10,000 times with the same bins as in Figure 11. We then average them together and average across 0 to produce a symmetric mean distribution. The distribution of correlation changes for each of the 10,000 cases is compared to the mean using relative entropy (DelSole & Tippett, 2007) as a measure of the difference in probability distributions. The distributions shown in Figure 11 are also compared to the mean random distribution. In each case, the distributions in Figure 11 due to the change in convective triggering is an extreme outlier, and the magnitude of relative entropy ranges from 2× (for LHF to MSE) to >10× (PBL height to convective cloud) larger than the largest attained by random sampling.

Globally, the greatest differences in spatially averaged correlations and spatial variability of differences over land are found between convection and convective available potential energy (CAPE, not shown). Dominant positive correlations across most of the continental areas become even stronger with the HCF trigger. Precipitation also becomes less correlated with CCC, as the model is less prone to frequent light rainfall. Other studies have shown that convective parameterizations tend to trigger clouds and convection too early in the day, cause frequent light rainfall, and generally perform more poorly than models at high enough resolution to permit clouds and convection directly (Dirmeyer et al., 2012; Hohenegger & Stevens, 2013; Kooperman et al., 2016; Pritchard & Somerville, 2009).

5. Discussion and Conclusions

We quantify as a function of space (across ice-free land areas of the globe) and time (as a function of the forecast lead time out to 60 days) the impact of land surface states on forecast skill in CFSv2. The three different treatments of land surface states allow us to estimate different levels of land surface impact. A maximum, albeit idealized, potential predictability of this model is determined by specifying the best possible analysis of land states throughout the forecast periods; best in that they are consistent coming from the reanalysis of the same model system featuring a parallel land surface analysis driven by observed meteorological forcing. This mode is a land-surface analog to Atmospheric Model Inter-comparison Project (AMIP)-type retrospective forecasts with specified observed sea surface temperatures. By comparing suites of forecasts with realistic land initialization in a true forecast mode (Same-Year IC) to randomized (Different-Year IC) land surface initialization, we can see the impact of evolving land surface states on forecast skill. Comparison of the two allows for assessment of the harvested predictability, realizing that there may be more harvestable predictability than is evident even with specified land states that is currently unrealizable due to model errors, biases, and imperfect monitoring and collection of data (especially regarding land surface states) assimilated in reanalyses and operational analyses.

We confirm with these experiments a long-held conjecture that the impact of the land surface on atmospheric forecast skill peaks in the interval between the short-term deterministic range of weather forecasts

largely determined by the initial state of the atmosphere and the realm of probabilistic seasonal forecasts (months and longer) where slowly evolving ocean states have a dominant contribution. Figure 3 shows that land surface impact on forecast skill peaks in the subseasonal range between about 5 days and 2 weeks, with a long tail of potential impact stretching out to 2 months or more depending on the validated variable and region. Thus, the land surface is shown to have key potential value in improving S2S forecasts. Recognition of the role of the land surface in predictions at S2S time scales has grown since GLACE-2; the land feedbacks component of the Land Surface, Snow and Soil Moisture Model Intercomparison Project (LS3MIP) revisits the topic of land surface contributions to prediction skill with a diagnostically focused multimodel community experiment (Van den Hurk et al., 2016).

This study uses a single climate model; as no model is perfect, it is possible that the full impact of the land surface on S2S time scales is being underestimated. A particular feature of the atmospheric component of CFSv2, also noted elsewhere (Abhik et al., 2017; Bombardi et al., 2015, 2016; Dirmeyer, 2013; Dirmeyer et al., 2018; Mo et al., 2012; Weber & Mass, 2017), is the unrealistic nature of simulated precipitation and its weak connection to land-atmosphere interactions. We see robust connections in CFSv2 between soil moisture, surface fluxes, and atmospheric properties both near the surface and through the daytime boundary layer. However, there is a sharp loss of signal in the last step from boundary layer properties to precipitation. Replacing the convective triggering parameterization, based on an arbitrary empirical relationship between the level of free convection and peak MSE, with one based on heating necessary to induce convective instability in the atmospheric profile, increases the linkage between land states and precipitation. However, the impact is largely confined to semiarid regions—the change in the parametrization is relatively minor compared to other convective criteria that were not altered.

We also see the effect of the change made to the root profiles between production of the CFS reanalysis and reforecasts to ameliorate surface warm biases over central North America. As noted previously (Dirmeyer & Halder, 2017; Roundy et al., 2014), this causes a wet surface bias over agricultural areas, especially noticeable over the midwestern United States, with excessive ET, very shallow boundary layers, and erroneously weak land-atmosphere coupling (Dirmeyer et al., 2018). Furthermore, snowpack and snowmelt biases in this model have some effect in April and May at high latitudes (Halder & Dirmeyer, 2017).

Despite these problems, our experiments suggest that CFSv2 is realizing most or all of the harvestable predictability from land surface states over some areas of the globe. There are also several unrealized sources of potential predictability. Errors in initial soil moisture states are likely in areas where precipitation is poorly observed (Koster et al., 2011; Oki et al., 1999). Land data assimilation, particularly utilizing remotely sensed soil moisture that has global coverage, has great potential to improve land surface initialization. Uncertainties and errors in parameter choices and model structure also contribute overall errors (Nearing et al., 2016), undoubtedly originating in both the land surface and atmospheric components of CFSv2. It must be recognized that all weather and climate models have problems in coupled land-atmosphere behavior that remain largely undiagnosed, due to two factors. One is the general lack of observational data needed to diagnose coupled land-atmosphere process errors in models (Dirmeyer et al., 2015). The other is the tradition of "stovepipe" model development wherein atmosphere and land surface models are developed in isolation from each other and at best lightly tuned after coupling. Pursuit of coupled, rather than piecemeal, land-atmosphere model development could speed improvements and help realize the unharvested predictability at S2S time scales.

Acknowledgments
This study was supported by a grant from the National Monsoon Mission, Ministry of Earth Sciences, Government of India (MM/SERP/COLA-GMU_USA/2013/INT-2/002) and National Oceanographic and Atmospheric Administration (NOAA) grant NA16OAR4310095. CPC Global Temperature data was provided by the NOAA/OAR/ESRL PSD, Boulder, Colorado, USA, from their Web site at https://www.esrl.noaa.gov/psd/. This work used resources of the Extreme Science and Engineering Discovery Environment (XSEDE); all CFSv2 model simulations were performed on the Texas Advance Computing Center's high-performance computing platform (Stampede) and model output data are stored on the long-term tape archival storage system (Ranch).

References

Abhik, S., Krishna, R. P. M., Mahakur, M., Ganai, M., Mukhopadhyay, P., & Dudhia, J. (2017). Revised cloud processes to improve the mean and intraseasonal variability of Indian summer monsoon in climate forecast system: Part 1: Cloud process on mean monsoon simulation. *Journal of Advances in Modeling Earth Systems*, *9*, 1002–1029. https://doi.org/10.1002/2016MS000819

Bombardi, R. J., Schneider, E. K., Marx, L., Halder, S., Singh, B., Tawfik, A. B., et al. (2015). Improvements in the representation of the Indian summer monsoon in the NCEP climate forecast system version 2. *Climate Dynamics*, *45*(9–10), 2485–2498. https://doi.org/10.1007/s00382-015-2484-6

Bombardi, R. J., Tawfik, A. B., Manganello, J. V., Marx, L., Shin, C.-S., Halder, S., et al. (2016). The heated condensation framework as a convective trigger in the NCEP Climate Forecast System version 2. *Journal of Advances in Modeling Earth Systems*, *8*, 1310–1329. https://doi.org/10.1002/2016MS000668

Chen, M., Shi, W., Xie, P., Silva, V. B. S., Kousky, V. E., Wayne Higgins, R., & Janowiak, J. E. (2008). Assessing objective techniques for gauge-based analyses of global daily precipitation. *Journal of Geophysical Research*, *113*, D04110. https://doi.org/10.1029/2007JD009132

Cheruy, F., Dufresne, J. L., Hourdin, F., & Ducharne, A. (2014). Role of clouds and land-atmosphere coupling in midlatitude continental summer warm biases and climate change amplification in CMIP5 simulations. *Geophysical Research Letters*, *41*, 6493–6500. https://doi.org/10.1002/2014GL061145

DelSole, T., & Tippett, M. K. (2007). Predictability: Recent insights from information theory. *Reviews of Geophysics*, *45*, RG4002. https://doi.org/10.1029/2006RG000202

Dirmeyer, P. A. (2011). The terrestrial segment of soil moisture-climate coupling. *Geophysical Research Letters*, *38*, L16702. https://doi.org/10.1029/2011GL048268

Dirmeyer, P. A. (2013). Characteristics of the water cycle and land–atmosphere interactions from a comprehensive reforecast and reanalysis data set: CFSv2. *Climate Dynamics*, *41*(3–4), 1083–1097. https://doi.org/10.1007/s00382-013-1866-x

Dirmeyer, P. A., Balsamo, G., & Peters-Lidard, C. D. (2015). Land-atmosphere interactions and the water cycle. In G. Brunet, S. Jones, & P. M. Ruti (Eds.), *Seamless prediction of the Earth system: From minutes to months* (pp. 145–154). Geneva, Switzerland: World Meteorological Organization.

Dirmeyer, P. A., Cash, B. A., Kinter, J. L., Jung, T., Marx, L., Satoh, M., et al. (2012). Simulating the diurnal cycle of rainfall in global climate models: Resolution versus parameterization. *Climate Dynamics*, *39*(1–2), 399–418. https://doi.org/10.1007/s00382-011-1127-9

Dirmeyer, P. A., Chen, L., Wu, J., Shin, C.-S., Huang, B., Cash, B. A., et al. (2018). Verification of land–atmosphere coupling in forecast models, reanalyses, and land surface models using flux site observations. *Journal of Hydrometeorology*, *19*(2), 375–392. https://doi.org/10.1175/JHM-D-17-0152.1

Dirmeyer, P. A., & Halder, S. (2016). Sensitivity of numerical weather forecasts to initial soil moisture variations in CFSv2. *Weather and Forecasting*, *31*(6), 1973–1983. https://doi.org/10.1175/WAF-D-16-0049.1

Dirmeyer, P. A., & Halder, S. (2017). Application of the land–atmosphere coupling paradigm to the operational Coupled Forecast System, version 2 (CFSv2). *Journal of Hydrometeorology*, *18*(1), 85–108. https://doi.org/10.1175/JHM-D-16-0064.1

Dirmeyer, P. A., Wu, J., Norton, H. E., Dorigo, W. A., Quiring, S. M., Ford, T. W., et al. (2016). Confronting weather and climate models with observational data from soil moisture networks over the United States. *Journal of Hydrometeorology*, *17*(4), 1049–1067. https://doi.org/10.1175/JHM-D-15-0196.1

Ek, M. B., Mitchell, K. E., Lin, Y., Rogers, E., Grunmann, P., Koren, V., et al. (2003). Implementation of Noah land surface model advances in the National Centers for Environmental Prediction operational mesoscale Eta model. *Journal of Geophysical Research*, *108*(D22), 8851. https://doi.org/10.1029/2002JD003296

Findell, K. L., & Eltahir, E. A. B. (2003). Atmospheric controls on soil moisture–boundary layer interactions. Part I: Framework development. *Journal of Hydrometeorology*, *4*(3), 552–569. https://doi.org/10.1175/1525-7541(2003)004<0552:ACOSML>2.0.CO;2

Findell, K. L., Gentine, P., Lintner, B. R., & Kerr, C. (2011). Probability of afternoon precipitation in eastern United States and Mexico enhanced by high evaporation. *Nature Geoscience*, *4*(7), 434–439. https://doi.org/10.1038/ngeo1174

Ford, T. W., Dirmeyer, P. A., & Benson, D. O. (2018). Evaluation of heat wave forecasts seamlessly across S2S time scales: Skill attribution and the role of land-atmosphere interactions. *NPJ Climate and Atmospheric Science*, *1*(1), 20. https://doi.org/10.1038/s41612-018-0027-7

Gentine, P., Holtslag, A. A. M., D'Andrea, F., & Ek, M. (2013). Surface and atmospheric controls on the onset of moist convection over land. *Journal of Hydrometeorology*, *14*(5), 1443–1462. https://doi.org/10.1175/JHM-D-12-0137.1

Griffies, S., Harrison, M. J., Pacanowski, R. C., & Rosati, A. (2004). A technical guide to MOM4, (Technical Report No. 5). NOAA/GFDL, Princeton, NJ. Retrieved from http://www.gfdl.noaa.gov/~fms

Halder, S., & Dirmeyer, P. A. (2017). Relation of Eurasian snow cover and Indian summer monsoon rainfall: Importance of the delayed hydrological effect. *Journal of Climate*, *30*(4), 1273–1289. https://doi.org/10.1175/JCLI-D-16-0033.1

Han, J., & Pan, H.-L. (2011). Revision of Convection and Vertical Diffusion Schemes in the NCEP Global Forecast System. *Weather and Forecasting*, *26*(4), 520–533. https://doi.org/10.1175/WAF-D-10-05038.1

Helfrich, S. R., McNamara, D., Ramsay, B. H., Baldwin, T., & Kasheta, T. (2007). Enhancements to, and forthcoming developments in the Interactive Multisensor Snow and Ice Mapping System (IMS). *Hydrological Procedure*, *21*(12), 1576–1586. https://doi.org/10.1002/hyp.6720

Hohenegger, C., & Stevens, B. (2013). Controls on and impacts of the diurnal cycle of deep convective precipitation. *Journal of Advances in Modeling Earth Systems*, *5*, 801–815. https://doi.org/10.1002/2012MS000216

Hong, S.-Y., & Pan, H.-L. (1996). Nonlocal boundary layer vertical diffusion in a medium-range forecast model. *Monthly Weather Review*, *124*(10), 2322–2339. https://doi.org/10.1175/1520-0493(1996)124<2322:NBLVDI>2.0.CO;2

Kirtman, B. P., Pegion, K., DelSole, T., Tippett, M., Robertson, A. W., Bell, M., et al. (2017). The subseasonal experiment (SubX). IRI Data Library. https://doi.org/10.7916/d8pg249h

Kooperman, G. J., Pritchard, M. S., Burt, M. A., Branson, M. D., & Randall, D. A. (2016). Robust effects of cloud superparameterization on simulated daily rainfall intensity statistics across multiple versions of the Community Earth System Model. *Journal of Advances in Modeling Earth Systems*, *8*, 140–165. https://doi.org/10.1002/2015MS000574

Kopp, T. J., & Kiess, R. B. (1996). The Air Force Global Weather Central snow analysis model. Preprints, 15th Conf. on Weather Analysis and Forecasting, Norfolk, VA, Amer. Meteor. Soc., 220–222.

Koster, R. D., Mahanama, S. P. P., Yamada, T. J., Balsamo, G., Berg, A. A., Boisserie, M., et al. (2010). Contribution of land surface initialization to subseasonal forecast skill: First results from a multi-model experiment. *Geophysical Research Letters*, *37*, L02402. https://doi.org/10.1029/2009GL041677

Koster, R. D., Mahanama, S. P. P., Yamada, T. J., Balsamo, G., Berg, A. A., Boisserie, M., et al. (2011). The second phase of the Global Land–Atmosphere Coupling Experiment: Soil moisture contributions to subseasonal forecast skill. *Journal of Hydrometeorology*, *12*(5), 805–822. https://doi.org/10.1175/2011JHM1365.1

Koster, R. D., Suarez, M. J., Higgins, R. W., & van den Dool, H. M. (2003). Observational evidence that soil moisture variations affect precipitation. *Geophysical Research Letters*, *30*(5), 1241. https://doi.org/10.1029/2002GL016571

Levine, P. A., Randerson, J. T., Swenson, S. C., & Lawrence, D. M. (2016). Evaluating the strength of the land–atmosphere moisture feedback in Earth system models using satellite observations. *Hydrology and Earth System Sciences*, *20*(12), 4837–4856. https://doi.org/10.5194/hess-20-4837-2016

Mo, K. C., Shukla, S., Lettenmaier, D. P., & Chen, L.-C. (2012). Do Climate Forecast System (CFSv2) forecasts improve seasonal soil moisture prediction? *Geophysical Research Letters*, *39*, L23703. https://doi.org/10.1029/2012GL053598

National Academies of Sciences, Engineering, and Medicine (U.S.) (Ed.) (2016). *Next generation Earth system prediction: Strategies for subseasonal to seasonal forecasts*. Washington, DC: The National Academies Press.

Nearing, G. S., Mocko, D. M., Peters-Lidard, C. D., Kumar, S. V., & Xia, Y. (2016). Benchmarking NLDAS-2 soil moisture and evapotranspiration to separate uncertainty contributions. *Journal of Hydrometeorology*, *17*(3), 745–759. https://doi.org/10.1175/JHM-D-15-0063.1

Oki, T., Nishimura, T., & Dirmeyer, P. (1999). Assessment of annual runoff from land surface models using Total Runoff Integrating Pathways (TRIP). *Journal of the Meteorological Society of Japan. Ser. II*, *77*(1B), 235–255. https://doi.org/10.2151/jmsj1965.77.1B_235

Olusegun, A. M., Muktar, A., Kabir, K. N., Adamu, I. A., & Abubakar, U. A. (2015). How a variable's partial correlation with other variable(s) can make a good predictor: The suppressor variable case. *International Journal of Advanced Statistics and Probability*, *3*(2), 210. https://doi.org/10.14419/ijasp.v3i2.5400

Pan, H.-L., & Wu, W.-S. (1995). Implementing a mass flux convective parameterization package for the NMC Medium-Range Forecast model (Note No. 409) (p. 40). NOAA.

Peters-Lidard, C. D., Houser, P. R., Tian, Y., Kumar, S. V., Geiger, J., Olden, S., et al. (2007). High-performance earth system modeling with NASA/GSFC's Land Information System. *Innovations in Systems and Software Engineering*, *3*(3), 157–165. https://doi.org/10.1007/s11334-007-0028-x

Pritchard, M. S., & Somerville, R. C. J. (2009). Assessing the diurnal cycle of precipitation in a multi-scale climate model. *Journal of Advances in Modeling Earth Systems*, *2*, 12. https://doi.org/10.3894/JAMES.2009.1

Roundy, J. K., Ferguson, C. R., & Wood, E. F. (2013). Temporal variability of land–atmosphere coupling and its implications for drought over the southeast United States. *Journal of Hydrometeorology*, *14*(2), 622–635. https://doi.org/10.1175/JHM-D-12-090.1

Roundy, J. K., Ferguson, C. R., & Wood, E. F. (2014). Impact of land-atmospheric coupling in CFSv2 on drought prediction. *Climate Dynamics*, *43*(1–2), 421–434. https://doi.org/10.1007/s00382-013-1982-7

Saha, S., Moorthi, S., Pan, H.-L., Wu, X., Wang, J., Nadiga, S., et al. (2010). The NCEP climate forecast system reanalysis. *Bulletin of the American Meteorological Society*, *91*(8), 1015–1058. https://doi.org/10.1175/2010BAMS3001.1

Saha, S., Moorthi, S., Wu, X., Wang, J., Nadiga, S., Tripp, P., et al. (2014). The NCEP climate forecast system version 2. *Journal of Climate*, *27*(6), 2185–2208. https://doi.org/10.1175/JCLI-D-12-00823.1

Santanello, J. A., Dirmeyer, P. A., Ferguson, C. R., Findell, K. L., Tawfik, A. B., Berg, A., et al. (2018). Land-Atmosphere Interactions: The LoCo Perspective. *Bulletin of the American Meteorological Society*. https://doi.org/10.1175/BAMS-D-17-0001.1, *99*(6), 1253–1272.

Tawfik, A. B., & Dirmeyer, P. A. (2014). A process-based framework for quantifying the atmospheric preconditioning of surface-triggered convection. *Geophysical Research Letters*, *41*, 173–178. https://doi.org/10.1002/2013GL057984

Tawfik, A. B., Dirmeyer, P. A., & Santanello, J. A. (2015a). The heated condensation framework. Part I: Description and Southern Great Plains case study. *Journal of Hydrometeorology*, *16*(5), 1929–1945. https://doi.org/10.1175/JHM-D-14-0117.1

Tawfik, A. B., Dirmeyer, P. A., & Santanello, J. A. (2015b). The heated condensation framework. Part II: Climatological behavior of convective initiation and land–atmosphere coupling over the conterminous United States. *Journal of Hydrometeorology*, *16*(5), 1946–1961. https://doi.org/10.1175/JHM-D-14-0118.1

Taylor, C. M., de Jeu, R. A. M., Guichard, F., Harris, P. P., & Dorigo, W. A. (2012). Afternoon rain more likely over drier soils. *Nature*, *489*(7416), 423–426. https://doi.org/10.1038/nature11377

Thomas, G., & O'Quigley, J. (1993). A geometric interpretation of partial correlation using spherical triangles. *The American Statistician*, *47*(1), 30. https://doi.org/10.2307/2684779

Trigo, I. F., Boussetta, S., Viterbo, P., Balsamo, G., Beljaars, A., & Sandu, I. (2015). Comparison of model land skin temperature with remotely sensed estimates and assessment of surface-atmosphere coupling. *Journal of Geophysical Research: Atmospheres*, *120*, 12,096–12,111. https://doi.org/10.1002/2015JD023812

Van den Hurk, B., Kim, H., Krinner, G., Seneviratne, S. I., Derksen, C., Oki, T., et al. (2016). LS3MIP (v1.0) contribution to CMIP6: The Land Surface, Snow and Soil moisture Model Intercomparison Project—Aims, setup and expected outcome. *Geoscientific Model Development*, *9*(8), 2809–2832. https://doi.org/10.5194/gmd-9-2809-2016

Vitart, F., Ardilouze, C., Bonet, A., Brookshaw, A., Chen, M., Codorean, C., et al. (2017). The subseasonal to seasonal (S2S) prediction project database. *Bulletin of the American Meteorological Society*, *98*(1), 163–173. https://doi.org/10.1175/BAMS-D-16-0017.1

Weber, N. J., & Mass, C. F. (2017). Evaluating CFSv2 subseasonal forecast skill with an emphasis on tropical convection. *Monthly Weather Review*, *145*(9), 3795–3815. https://doi.org/10.1175/MWR-D-17-0109.1

Williams, I. N., Lu, Y., Kueppers, L. M., Riley, W. J., Biraud, S. C., Bagley, J. E., & Torn, M. S. (2016). Land-atmosphere coupling and climate prediction over the U.S. Southern Great Plains. *Journal of Geophysical Research: Atmospheres*, *121*, 12,125–12,144. https://doi.org/10.1002/2016JD025223

Xie, P., & Arkin, P. A. (1997). Global precipitation: A 17-year monthly analysis based on gauge observations, satellite estimates, and numerical model outputs. *Bulletin of the American Meteorological Society*, *78*(11), 2539–2558. https://doi.org/10.1175/1520-0477(1997)078<2539:GPAYMA>2.0.CO;2

Xie, P., Chen, M., Yang, S., Yatagai, A., Hayasaka, T., Fukushima, Y., & Liu, C. (2007). A gauge-based analysis of daily precipitation over East Asia. *Journal of Hydrometeorology*, *8*(3), 607–626. https://doi.org/10.1175/JHM583.1

Zeng, D., & Yuan, X. (2018). Multiscale land–atmosphere coupling and its application in assessing subseasonal forecasts over East Asia. *Journal of Hydrometeorology*, *19*(5), 745–760. https://doi.org/10.1175/JHM-D-17-0215.1

Zhang, L., Dirmeyer, P. A., Wei, J., Guo, Z., & Lu, C.-H. (2011). Land–atmosphere coupling strength in the Global Forecast System. *Journal of Hydrometeorology*, *12*(1), 147–156. https://doi.org/10.1175/2010JHM1319.1

Zhang, Y., Klein, S. A., Fan, J., Chandra, A. S., Kollias, P., Xie, S., & Tang, S. (2017). Large-eddy simulation of shallow cumulus over land: A composite case based on ARM long-term observations at its Southern Great Plains site. *Journal of the Atmospheric Sciences*, *74*(10), 3229–3251. https://doi.org/10.1175/JAS-D-16-0317.1